DISCLAIMER

This document was prepared as an account of work sponsored by the United States Government. While this document is believed to contain correct information, neither the United States Government nor any agency thereof, nor the Regents of the University of California, nor any of their employees, makes any warranty, express or implied, or assumes any legal responsibility for the accuracy, completeness, or usefulness of any information, apparatus, product, or process disclosed, or represents that its use would not infringe privately owned rights. Reference herein to any specific commercial product, process, or service by its trade name, trademark, manufacturer, or otherwise, does not necessarily constitute or imply its endorsement, recommendation, or favoring by the United States Government or any agency thereof, or the Regents of the University of California. The views and opinions of authors expressed herein do not necessarily state or reflect those of the United States Government or any agency thereof or the Regents of the University of California.

Current Titles

National Center for Electron Microscopy

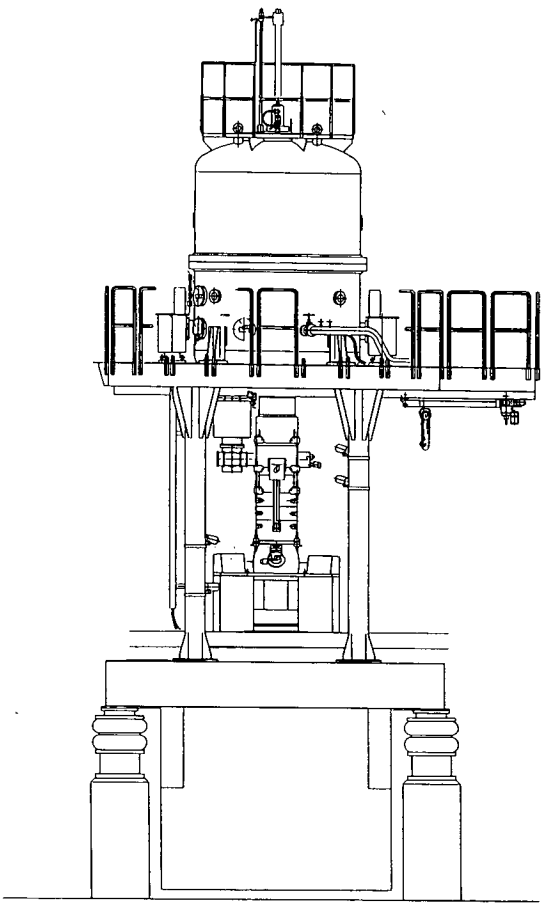

REFERENCE COPY
Does Not
Circulate
Bldg. 50 Library.
Copy 1
PUB-719

April 1994

National Center for Electron Microscopy
U.C. Lawrence Berkeley Laboratory
1 Cyclotron Rd. Building 72
Berkeley CA 94720

National Center for Electron Microscopy
U.C. Lawrence Berkeley Laboratory
1 Cyclotron Rd. Building 72
Berkeley CA 94720

Please send a reprint of the paper(s):

Number	Author(s)	Title

Name_____ Date_____

Affiliation_____

Address_____

_____

Please send a reprint of the paper(s):

Number	Author(s)	Title

Name_____ Date_____

Affiliation_____

Address_____

_____

Current Titles

National Center for Electron Microscopy
Lawrence Berkeley Laboratory
University of California
Berkeley, California 94720

April 1994

PUB-719

The NCEM is supported by the Director, Office of Energy Research, Office of Basic Energy Sciences, Materials Sciences Divison of the U.S. Department of Energy under Contract No. DE-AC03-76SF00098.

This booklet is published for those interested in current research being conducted at the National Center for Electron Microscopy. The NCEM is a DOE-designated national user facility and is available at no charge to qualified researchers. Access is controlled by an external steering committee. Interested researchers may contact Gretchen Hermes at (510) 486-5006 or address below for a User's Guide.

Copies of available papers can be ordered from:

Theda Crawford
National Center for Electron Microscopy
Lawrence Berkeley Laboratory
One Cyclotron Rd., MS72
Berkeley, California, USA 94720

Articles are listed alphabetically by journal.

Legend:

Number = publication number

R = Reprints P = Preprints No = None available

recycled paper

Pub475Rev.93 P

NCEM User's Guide

User's guide to the National Center for Electron Microscopy, Lawrence Berkeley Laboratory, University of California, Berkeley.

34063 R

C.P. Luo, U. Dahmen, and K.H. Westmacott

Morphology and Crystallography of Cr Precipitates in a Cu-0.33 wt.% Cr Alloy

Acta Met. et Mat. (in press). LBL-30872 revision.

The morphology and crystallography of Cr-rich precipitates in a Cu-0.33wt.%Cr alloy have been investigated in detail by transmission electron microscopy. The precipitates were lath-shaped and well-faceted. Their orientation relationship with the matrix was identical for all precipitates observed. One set of close-packed planes in the two phases were exactly parallel, with the close packed directions enclosing an angle of 0.5°, a systematic deviation of 0.5° from the Kurdjumov-Sachs orientation relationship, or 5.76° from Nishiyama-Wassermann. This relationship produced an invariant line strain transformation. The lath axis was aligned precisely with the high-index [-5, 6,-1]f invariant line direction, located at the intersection of the close-packed planes (111)f||(110)b with the cone of unextended lines. The dominant interface facet was found to be (3.1 3.5 5.5)f or ~2° away from (335)f. All crystallographic measurements were in excellent agreement with the predictions from the invariant line strain model for the Bain lattice distortion with a lattice parameter ratio af/ab=1.264, assuming a pair of parallel close packed planes, but inconsistent with predictions of the phenomenological theory of martensitic transformationss.

PUB658 P

M.A. O'Keefe and R. Kilaas

NCEMSS User's Guide

This manual describes the NCEMSS computer program for simulation of HRTEM images. The program is designed to run on any VaxStation running VWS (uis) or Dec-Windows with either VMS or Ultrix as the operating system. It can be obtained from the NCEM on magnetic media, or down-loaded by using Telnet to login to the NCEM VaxStation ORAC.LBL.GOV using the ID of ANONYMOUS.

34812 R

R.W. Beye and R. Gronsky

Novel Phases in the Oxidation of γ-Titanium Aluminum

Acta Met et Mat., Vol. 42, #4 p.1373 (1994).

This paper concentrates on the high temperature oxidation of g-titanium aluminum. Samples of Ti-47.5 at .% Al were subjected to a 1000° C oxygen environment for various times and subsequently examined by Auger Electron Spectroscopy (AES), X-ray Diffraction (XRD), Scanning Electron Microscopy (SEM), and optical microscopy. AES proved to be useful in identifying oxygen scavenging by Ti_3Al and also in examining a subscale Al depletion layer, which was found to contain two previously unreported phases, tentatively identified as $Ti_{10}Al_6O$, and $Ti_{10}Al_6O_2$. These phases enabled an updated description of γ-titanium aluminum oxidation at temperatures from room temperature to above 1100°C.

---

un-numbered No

P.M. Vasconcelos, H.-R. Wink, and C. Echer

In-situ Study of the Thermal Behavior of Cryptomelane by High-Voltage and Analytical Electron Microscopy

American Mineralogist, Vol. 79, p.81 (1994).

Scanning electron microscope (SEM) and transmission electron microscope (TEM) studies show that cryptomelane and Cu-rich cryptomelane crystals from weathering profiles in Brazil range from 10 to 200 nm in diameter and have aspect ratios of 1:10 to 1:100 between the long and short dimensions. Acicular crystals identified in hand specimen and in the scanning electron microscope are often composed of bundles of fibers elongated along the c axis (tetragonal) or the b axis (monoclinic). In-situ heating with a high-voltage transmission electron microscope (HVEM) and an analytical electron microscope (AEM) indicates that upon heating in vacuum cryptomelane crystals begin to transform into a mixed hausmannite and manganosite phase at 648° C, and manganosite begins to form at 620° C. Cu-rich cryptomelane also loses K and exsolves native copper upon heating, suggesting that Cu occupies the same site (the A site) as K. Similar mineral transformations are observed when the same samples are heated in air, although the transformations occur at higher temperatures than those observed in vacuum.

---

un-numbered No

E.E. Fullerton, W. Cao, G. Thomas, I.K. Schuller, M.J. Carey, and A.E. Berkowitz

Quantitative Characterization of Epitaxial Superlattices by X-ray Diffraction and High Resolution Electron Microscopy

Appl. Phys. Lett., 63 (4), p.482 (July, 1993).

Quantitative x-ray diffraction (XRD) and high resolution electron microscopy (HREM) have been applied to the analysis of an epitaxial CoO/NiO superlattice. This example shows that the qualitative information determined directly from a XRD spectrum or HREM image is limited and can even be misleading. However, by a combination of quantitative intensity measurements and structural modeling, a detailed quantitative characterization of the superlattice structure is possible.

un-numbered No

S.H. Risbud, L.-C. Liu, and J.F. Shackleford

Synthesis and Luminescence of Silicon Remnants Formed by Truncated Glassmelt-Particle Reaction

Appl. Phys. Lett., 63, (12), p.1648 (1993).

We have obtained nanometer sized silicon remnants sequestered in glass matrices by terminating the reaction of pure silicon powders dispersed in the viscous melt at a temperature of 1400° C. Repeated use of this truncated melt-particle reaction process dilutes the amount and size of silicon remnants, and bulk samples containing nanosize silicon crystallites embedded in a glass matrix were eventually obtained. These quantum dot sized silicon-in-glass materials emit greenish luminescence with peak wavelengths from ~480 to 530 nm, considerably shorter than the reddish luminescence (at about 700-850 nm) observed in porous silicon structures prepared by electrochemical etching techniques; upon complete digestion of Si particles by the melt, the luminescence peaks disappear. Since our silicon-in-glass preparation method does not involve etching, the origin of the luminescence is not likely to be due to Si-O-H compounds (e.g., siloxene) postulated recently. The location of the luminescence peaks and the observed silicon crystallite size suggest quantum confinement leading to a widened silicon band gap arising from remnants in the glass matrix smaller than the exciton diameter of bulk silicon (10 nm).

---

un-numbered R

K.M. Krishnan, Y. Honda, Y. Hirayama, and M. Futamoto

Microstructure and Epitaxy of c-axis Oriented Single Crystal Cobalt Films Grown on Rigid Underlayers

Appl. Phys. Lett., Vol. 64, (12), p.1499 (1994).

We have established the conditions to grow *c*-axis oriented Co Films on mica substrates and characterized their crystallography and microstructure in detail. In particular, these films are single crystal, c-axis oriented, Co_{hcp} and are grown epitaxially by *e*-beam evaporation on either Ti or Ru underlayers.

un-numbered No

S. Im, J. Washburn, R. Gronsky, N.W. Cheung, K.M. Yu, and J.W. Ager

Optimization of Ge/C Ratio for Compensation of Misfit Strain in Solid Phase Epitaxial Growth of SiGe Layers

Appl. Phys. Letts., Vol. 63, (19), p.2682 (1993).

In order to study the strain-compensation effect by C atoms in solid phase epitaxial (SPE) growth of SiGe alloy layers, C sequential implantation was performed in [100] oriented Si substrates with various doses after high dose Ge implantation. When the nominal peak concentration of implanted C was over 0.55 at% in the present sample series, misfit dislocation generation in the epitaxial layer was considerably suppressed. A SiGe alloy layer with 0.9 at% C peak concentration under a 12 at% Ge peak shows the greatest improved crystallinity compared to layers with smaller C peak concentrations. The experimental results, combined with a simple model calculation, indicate that the optimum Ge/C ratio for strain compensation is between 11 and 22.

35116 No

D. Loretto, F.M. Ross, C.A. Lucas, and G.C.L. Wong

Direct Observation of Interface and Surface Steps in Epitaxial Films by Dark-Field Transmission Electron Microscopy

Applied Physics Letters (submitted 2/94).

We have used dark-field transmission electron microscopy to investigate <5 nm thick CaF_2 films grown on Si(111) by molecular beam epitaxy. Images formed with CaF_2[111] reflections exhibit contrast at 1/3[111] high steps at the CaF_2 surface and at the CaF_2/Si interface over large (>100 μm^2), statistically significant areas. Direct evidence for step flow growth in CaF2 has been obtained.

33539 No

M.A. Brewer and K. Krishnan

Effects of Substrate Surface Preparation on Diamond Nucleation in Chemical Vapor Deposition

Applied Physics Letters (accepted, 1994).

Microwave plasma CVD diamond was deposited on silicon substrates with different surface preparations to evaluate the parameters that affect nucleation density and quality. (100) silicon wafers were polished or randomly distributed with 1-μm diamond, 0.2-μm SiC or 0.8-μm Si_3N_4 and the resulting nucleation density after 60-min. depositions compared. Diamond resulted in the best nucleation enhancement, then Si_3N_4 and SiC, respectively. Given that SiC was found to be an interfacial layer between silicon and diamond films by some experimenters, it was surprising that SiC particles did not nucleate diamond. Other silicon substrates were scratched with a tungsten scribe to create surface defects without leaving residual powder particles. Nucleation was not enhanced on these substrates. These measurements support an earlier result that diamond nanocrystallites embedded in the substrate during its preparation are the preferred sites for nucleation.

33574 P

S. Im, J. Washburn, R. Gronsky, N.W. Cheung and K.M. Yu

Defect Control During Solid Phase Epitaxial Growth of SiGe Alloy Layers

Applied Physics Letters, Vol. 63 (7) p.929 (1993).

A systematic study of the processing procedures required for minimizing structural defects generated during the solid phase epitaxial (SPE) growth of SiGe alloy layers is described. It includes high dose Ge implantation into Si at liquid nitrogen temperature (LNT), sequential carbon implantation, and an 800° C anneal. The LNT implantation step considerably reduces the density of end-of-range (EOR) defects relative to that found in SPE grown SiGe layers implanted at room temperature, while the sequential implantation of carbon ions before annealing effectively suppresses the formation of stacking faults that are found to form at a threshold peak concentration of about 6 at %Ge in the absence of carbon.

un-numbered No

W.G. Hirt, H.-R. Wenk, and J.R. Boles

Albitization of Plagioclase Crystals in the San Joaquin Basin, California, and the Gulf Coast, Texas: A TEM/AEM Study

Geological Soc. of Am. Bulletin, Vol. 105, p.708 (1993).

Conventional Transmission Electron Microscopy (CTEM) and Analytical Electron Microscopy (AEM) studies of partially albitized plagioclase crystals taken from drill cores from the Stevens sandstone (Miocene), San Joaquin, California, and the Frio Formation (Oligocene), Gulf Coast, Texas, reveal that replacement of Ca-rich plagioclase cores by nearly pure albite (Al_{96}-Ab_{100}) occurs along submicroscopic (~15 nm wide) ***en echelon*** (001) and (1110) cleavages. The cleavages are the result of changes in the localized stress regime created by dissolution of adjacent phases. Photomicrograph show albite-lined brittle cleavage crosscutting albitized semibrittle fractures. Such crosscutting relationships can be explained by a reduction in effective stress associated with the albitization process. On a macroscopic scale, this reduction in effective stress implies that the transition from hydrostatic to lithostatic pressure is discontinuous.

34587 P

N. Thangaraj, C. Echer, K.M. Krishnan, R.F.C. Farrow, R.F. Marks, and S.S.P. Parkin

Giant Magnetoresistance and Microstructural Characteristics of Epitaxial Fe-Ag and Co-Ag Granular Thin Films

Journal of Applied Physics (in press, 1994).

Giant magnetoresistance (GMR) and its relationship with the microstructure in phase separated FeAg and CoAg granular thin films grown epitaxially on (001) NaCl substrates by MBE, were studied by transmission electron microscopy (TEM) and magnetic characterization techniques. The influence of microstructural features such as growth twins, Fe and Co phase distribution, grain size distribution and orientation on the observed magnetic properties of these granular alloy films will be discussed.

35393 No

U. Dahmen, S. Paciornik, I.G. Solorzano, and J.B. Vandersande

HREM Analysis of Structure and Defects in a Sigma 5 (210) Grain Boundary in Rutile

Interface Science (submitted 3/14/94).

The structure of a Sigma 5 (210) boundary in rutile was investigated by high resolution electron microscopy (HREM). The boundary was stepped with an average inclination of about 5° from the symmetrical (210) plane. The steps were associated with 1/5[210] DSC lattice dislocations accommodating a deviation of about 2° from the exact Sigma 5 misorientation of 53.1°, and resulting in a misorientation of 51°. The boundary topography, the location of structural units and the local symmetry were determined using pattern recognition techniques. Flat terraces between steps had a periodic Sigma 5 (210) structure which exhibited mirror glide symmetry. Image simulations showed best agreement with experimental images for a model structure with a rigid body shift of 0.21nm parallel, and a 0.10nm volume contraction normal to the interface. This structure requires a high density of defects or an excess of Ti ions, presumably of lower oxidation state.

32819 R, P

B. Zhang, K.M. Krishnan, C.H. Lee and R.F.C. Farrow

Magnetic Anisotropy and Lattice Strain in Co/Pt Multilayers

Journal of Applied Physics, Vol. 73, p.10, (15 May 1993).

We report on the correlation between perpendicular anisotropy and in-plane lattice strain in Co/Pt multilayers. $(Co_x/Pt_y)n$ samples, where x, y are the thickness of the individual Co and Pt layers and n is the number of repeats were prepared by Molecular Beam Epitaxy and studied by means of polar Magneto-Optic Kerr effect and transmission electron microscopy. Kerr rotation data and electron diffraction experiments show that the largest perpendicular anisotropy and square hysteresis loop occur when x = 3Å while the Pt layers are subjected to about -2% in-plane strain. As Co thickness increases, Co and Pt layers gradually lose coherency and the magnetic anisotropy goes from perpendicular to planar. This is accompanied by a relaxation of lattice strain in both Co and Pt layers. The close relationship between magnetic anisotropy and lattice strain can be explained as magneto-elastic anisotropy or stress anisotropy effect due to lattice mismatch between the adjacent epitaxial layers.

35150 No

T. Komaya, A.T. Bell, A. Weng-Sieh, R. Gronsky, F. Engelke, T.S. King, and M. Pruski

The Influence of Metal-Support Interactions on the Accurate Determination of Ru Dispersion for Ru/TiO_2

Journal of Catalysis (submitted 2/4/94)

Titania-supported Ru catalysts have been characterized by TEM, ^1H NMR, and H_2 chemisorption to determine the metal particle size, the fraction of the metal surface available for H_2 chemisorption, and the H_2 adsorption capacity of the catalyst, as functions of the reduction temperature. TEM micrographs show that as the reduction temperature rises from 573 K to 773K the average particle size of Au remains the same but the surface of the particles is covered to an increasing extent by an amorphous layer of titania. Quantitative estimates of the fraction of the Au particle surface available for H_2 chemisorption were obtained by ^1H NMR. The NMR spectra also show that a fraction of the adsorbed H_2 spills over onto the support and that as a consequence measurements of total H_2 chemisorption overestimate the number of Ru sites available for H_2 adsorption. The implications of these results for the correct calculation of Ru dispersion and the determination of turnover frequencies for reactions carried out over Ru/TeO_2 are discussed.

35396 No reprints

R. Kilaas, S. Paciornik, A.J. Schwartz, and L.E. Tanner

Quantitative Analysis of Atomic Displacements in HRTEM Images

Journal of Computer Assisted Microcopy (submitted 3/24/94).

In images of imperfect crystals it is important to determine the positions of atoms away from the perfect lattice positions. Although atoms are not always individually resolved, there are many systems where atoms are imaged as either white or black "dots". In these systems, the localization of atoms is made by searching for peaks in the image. However, practical problems are often encountered using peak finding algorithms found in available software packages. This paper describes a method for quantifying the atomic displacements in High Resolution TEM images to high accuracy. The method treats common problems associated with intensity saturation, noise and spurious peaks. The method has been applied to a HRTEM image of a modulated structure, $Ti_{50}Pd_{42}Cr_8$ where the atoms are displaced from the perfect lattice sites by a "frozen" displacement wave. In addition to describing the peak finding algorithm and the refinement of peak positions to sub-pixel accuracy, the paper also shows how spurious peaks can be eliminated and how missing peaks can be reintroduced.

35440 No

T. Komaya, A.T. Bell, Z. Weng-Sieh, R. Gronsky, F. Engelke, T.S. King, and M. Pruski

Effects of Dispersion and Metal-Metal Oxide Interactions on Fischer-Tropsch Synthesis over Ru/TiO_2 and TiO_2-Promoted Ru/SiO_2

Journal of Catalysis (submitted 4/2/94).

The activity of Ru/TiO_2 and TiO_2-promoted Ru/SiO_2 catalysts for Fisher-Tropsch synthesis have been investigated. The Ru dispersion of these catalysts was determined by TEM and the fraction of the Ru surface available for H_2 adsorption was determined by ^1H NMR. Even after low-temperature reduction, the surface of titania-containing catalysts is covered by titania to a substantial degree. The specific activity and selectivity of these catalysts is dominated by the interactions occurring between the Ru particles and the titania overlayer. As the fraction of the Ru particle surface covered by titania increases, the turnover frequency for CO consumption passes through a maximum, while that for methane formation decreases monotonically. The probability for chain growth and the olefin to paraffin ratio of the products increase with increasing titania coverage. These trends are attributed to the effects of the titania overlayer on the catalytic properties of Ru.

34447 No

W.B. Knowlton, K.M. Itoh, J.W. Beeman, J.B. Emes, D. Loretto, and R.E. Haller

Ge-Au Eutectic Bonding of Ge {100} Single Crystals

Journal of Low Temperature Physics, Vol. 93 p.343 (1993).

We present preliminary results on the eutectic bonding between two {100} Ge single crystal surfaces using thin films of Au ranging from 900Å/surface to 300Å/surface and Pd (10% the thickness of Au). Following bonding, plan view optical microscopy (OM) of the cleaved interface of samples with Au thicknesses <500Å/surface show a eutectic morphology more conducive to phonon transmission through the bond interface. High resolution transmission electron microscopy (HRTEM) cross sectional interface studies of a 300Å/surface Au sample show <100> epitaxial growth of Ge. In sections of the bond, lattice continuity of the Ge is apparent through the interface. TEM studies also reveal <110> heteroepitaxial growth of Au with a Au-Ge lattice mismatch of less than 2%. Eutectic bonds with 200Å/surface Au have been attained. An optical polishing technique for Ge has been optimized to insure intimate contact between the Ge surfaces. Interferometry analysis of the optically polished Ge surface shows that surface height fluctuations lie within ≠150Å across an interval of 1mm. Characterization of phonon transmission through the interface is discussed with respect to low temperature detection of ballistic phonon.

35165 No

Z. Weng-Sieh, P. Krulevitch, R. Gronsky, and G.C. Johnson

Stress Induced Formation of Structural Defects on the {311} Planes of Silicon

Journal of Mat. Res. (submitted 1/93).

Structural defects occurring on the {311} planes of single crystal silicon have been observed near the bottom oxide corner in silicon-on-insulator structures formed by selective epitaxial growth. These {311} defects exhibit a preferential orientation and are clustered near the silicon/silicon dioxide interface. This new observation provides an opportunity to study the mechanism of {311} defect generation in a system with discernible microstructure and stress state. High resolution electron microscopy combined with analytical and numerical three-dimensional stress modeling are used to show the dependence of these defects on the local stress field, and to establish their origin in terms of the homogeneous dislocation nucleation model (J. Vanhellmont et al).

---

un-numbered No

W.W. Milligan, S.A. Hackney, M. Ke and E.C. Aifantis

In Situ Studies of Deformation and Fracture in Nanophase Materials

Journal of Nanostructural Materials, Vol. 2, p.267 (1993).

Nanocrystalline gold (8-25 nm grain size) and gold/silicon nanocomposites were prepared by sputtering and then strained to fracture in a transmission electron microscope. *In situ* and *post mortem* analyses revealed that the nanophase gold films were ductile, and significant plasticity was associated with fracture. Observations of pore formation, as well as a strain-rate effect on deformation behavior and direct lattice imaging of deformation, all indicated that the deformation occurred by diffusion-based mechanisms. Fracture was intergranular, but not brittle. Gold/silicon nanocomposites containing large volume fractions of brittle, amorphous Si and nanocrystalline gold precipitates exhibited behavior indicating significant toughness.

un-numbered No

A.F, Pajares, F. Guiberteau, K.H. Westmacott, and A. Dominguez-Rodriguez

TEM Characterization of Indented Polycrstalline Y-PSZ

Journal of Mat. Sci., 28, p.6709 (1993).

The microstructural characterization of indented Y-PSZ polycrystals has been investigated by TEM. The observations show two different regions associated with the indent: a large core with a high density of monoclinic particles transformed from the initial tetragonal variant, and an inner core region with a high density of dislocations. The core region can be correlated with previous observations of a crack exclusion zone.

---

un-numbered No

T. Mitchell, Jr., L.C. De Jonghe, W.J. Moberly-Chan, and R.O. Ritchie

Silicon Carbide Platelet/Silicon Carbide Composites

Journal of the American Ceramic Soc., (submitted 1994).

Alpha-silicon carbide platelet/beta-silicon carbide composites have been produced in which the individual platelets were coated with an aluminum oxide layer. Hot pressed composites showed a fracture toughness as high as 7.2 Mpa.$m^{1/2}$. The experiments indicated that the significant increase in fracture toughness is mainly the result of crack deflection and accompanying platelet pull out. The coating on the platelets also served to prevent the platelets from acting as nucleation sites for the alpha to beta phase transformation, so that advantageous microstructure remains preserved during high temperature processing.

un-numbered No

S.A. Hackney

An Analysis of Morphological Instabilities at the Initiation of the Eutectoid Transformation Using a Kinetic Analogue

Journal of the Mechanical Behavior of Metals, Vol. 5, #1, p.11 (1993).

The study of the equilibrium structure of two component solids at constant pressure is often carried out with the use of a stability diagram where temperature and composition are the variables. Such diagrams often called phase diagrams, indicate the range of temperature and composition where thermodynamic phases are observed to be stable.

35164 No

U. Dahmen

A Comparison Between Three Simple Crystallographic Principles of Precipitate Morphology

Met. Trans (in press, 1994).

The connection between the optimum shape and orientation relationship of precipitates in a solid is examined. Three simple criteria for precipitate morphology are compared and illustrated schematically: the principle that precipitate dimensions tend to be inverse to the magnitude of the transformation strain; the postulate that precipitates are bounded by unrotated planes (eigenplanes); and the proposal that interfaces are parallel to the planes of three independent dislocation loop arrays necessary to accommodate the transformation strain completely. These principles are illustrated for different orientation relationships and it is shown that special features are displayed by invariant line precipitates. The implications of these criteria for experimental studies of precipitate morphologies are discussed and their predictions compared with results from a recent study of lath-shaped precipitates in Cu-Cr alloys.

---

un-numbered No

J. Liu, M.L. Dass and R. Gronsky

Transmission Electron Microscopy Study of Two Dimensional Semiconductor Device Junction Delineation by Chemical Etching

Journal of Vacuum Sci. & Tech., Vol. B-12, #1, p.353 (1994).

Quantitative chemical delineation of both n+ and p+ junctions in silicon-based integrated circuits has been achieved and monitored with respect to etching time, temperature, and ultraviolet illumination, using samples prepared by a new planar polishing technique for uniform initial flatness. Junction depths and dopant profiles obtained from cross-sectional transmission electron microscopy images are compared and cross-calibrated with both secondary ion mass spectrometry and spreading resistance profiling, confirming that dopant concentrations of 10^{17} cm^{-3} are detected and laterally mapped with better than 10 nm spatial resolution.

33607 P

J.B. Liu, B.M. Tracy and R. Gronsky

Selected Area Polishing for Precision TEM Sample Preparation

Microscopy Research and Tech., Vol. 26, p.162 (1993).

A selected area mechanical polishing technique has been developed to improve the precision of cross-sectional TEM sample preparation, based upon the early work of Benedict et al. (1990). TEM samples were made from a preselected section through the middle of a 1 μm wide band of transistors extending laterally for more than 1 mm by precise control over the plane of polish with a corresponding reduction in sample preparation time. To illustrate the application of this technique, a uniformly-thin, electron transparent TEM sample of a single, specific, failed transistor is obtained from a 4 mm by 10 mm device array.

un-numbered No

M.J. Witcomb and U. Dahmen

A Method for Jet Polishing Two-Phase Materials

Microscopy Research and Technique (submitted 4/4/94).

A two-stage jet polishing technique is described which, utilising the effects of the characteristic current-voltage behavior of electropolishing solutions, can produce excellent TEM foils of relatively course two-phase materials.

35332 R

U. Dahmen

Evolution of Ge Precipitate Morphology in Al

MRS Bulletin (submitted 3/9/94).

In-situ high voltage electron microscopy has been employed to study shape transformations of Ge precipitates in an Al-Ge alloy. During temperature cycling, lath-shaped Ge precipitates with a low-symmetry orientation relationship dissolved and regrew at their ends, becoming rounded during dissolution and sharply faceted during regrowth. These observations illustrate the strong dependence of growth mechanism and kinetics on the interface structure and are discussed in terms of a roughening transformation similar to that known for solid surfaces. These mechanisms have strong implications for the control of precipitate morphologies and the stability of interfaces in device structures.

35524 No

F.M. Ross

Materials Science in the Electron Microscope

MRS Bulletin (June, 1994, in press).

Techniques which combine real time image acquisition with high spatial resolution have contributed to our understanding of a remarkably diverse range of physical phenomena. In this issue we will present recent advances in materials science which have been made using the techniques of transmission electron microscopy (TEM), including holography, scanning electron microscopy (SEM), low energy electron microscopy (LEEM), and high voltage electron microscopy (HVEM).

34607 R

U. Dahmen

High Resolution Electron Microscopy of Interfaces

MSA Bulletin, Vol. 24, #1, p.341 (1993).

This paper reviews recent progress in high resolution electron microscopy (HREM) of internal interfaces in solids. A brief summary of generic interface features of interest is followed by specific examples of HREM investigations of grain boundaries and heterophase interfaces. Features of interest include interface roughness, rigid body displacements, faceting, steps or ledges, elastic displacement fields, atomic bonding, composition gradients and localized atomic relaxation into structural units. Two types of analysis, direct interpretation and comparison with image simulations are applicable to different types of interface characteristics. Critical issues of current importance and recent developments in technique are outlined for asymmetrical and symmetrical grain boundaries and for metal-semiconductor and metal-ceramic interfaces.

33829 R.

J. Turner, M.A. O'Keefe and S. Paciornik

Image Processing to Extract Line Information from Micrographs

MSA Proc. 51, p.208 (1993).

In processing microscope images, it is sometimes important to be able to extract the lengths and directions of linear features. For example, in characterizing transmission electron microscope images of faceted grain boundaries, the desired information is the length of grain boundary lying along each direction. In order to measure grain boundary lengths automatically, micrographs must be digitized and the linear features (e.g. the grain boundaries) binarized and reduced to a single pixel width. Then the problem requires finding two simple parameters for each line in the image: its direction and number of pixels. A new approach to this problem is to project the intensities of the source image in all possible directions, and to collect the projection results into a new two-dimensional "image" with one dimension representing the projection direction. This new image is called the sinogram of the source image. Each peak in the sino-gram represents a line, with one coordinate of the peak equal to the line's angle, and the other to its position. Intensities of peaks in the sinogram are equal to the numbers of pixels in the equivalent lines.

33926 No

R. Kilaas

Image Simulation in Electron Microscopy

MSA Proc. 51, p.542 (1993).

The theoretical calculation of High Resolution Transmission Electron Microscopy (HRTEM) images has become a routine operation due largely to the existence of several commercially available computer programs. Associated with these "black box" calculations, exists a danger coming from the ease with which the programs can be used to produce images without any understanding of the underlying physical principles and approximations used in the calculations. While hopefully, the majority of users of image simulation take the care to understand the limitations of the technique, there are several basic principles that must be understood in order to use the technique within the limits of its applicability.

33821 R

S. Paciornik, R. Kilaas, U. Dahmen and M.A. O'Keefe

A Method for Direct Measurements of Specimen Noise in HREM Images

MSA Proc. 51, p. 458 (1993)

Quantitative analysis of defect structures is often seriously limited by specimen noise due to contamination or oxide layers on the surfaces of a thin foil. Image simulations illustrate that, in the absence of specimen noise (under optimum conditions and subject to limitations not discussed here), a small displacement of a single atomic column can be imaged faithfully and measured directly from the image. However, the accuracy of such a measurement is compromised by specimen noise. The present method for noise assessment is based on the average displacement of image intensity peaks due to contamination or oxide layers. To determine this average displacement, it is necessary to extract the image peak positions and compare them with a set of reference peak positions. The list of peak positions is obtained by finding the center of mass of intensity peaks located near atomic positions in the experimental image. Then a reference list is created by performing a least-squares fit of a 2D lattice upon the positions of the first list. Assuming a perfect periodic lattice, this reference list approximates the positions of intensity peaks in the absence of noise. The root mean square (rms) deviation between the lists is used as a direct measure of the noise in the image. The method described here allows a clear assessment of the specimen noise-imposed limitations to structural defect analysis in simple materials.

33822 R

J.O. Malm and M.A. O'Keefe

Using Convergence and Spread of Focus Parameters to Model Spatial and Temporal Coherence in HRTEM Image Simulations

MSA Proc. 51, p.974 (1993).

In all HRTEM images, the incident electron beam suffers from the effects of limited spatial and temporal coherence. These effects produce a smearing of the image, and provide the ultimate limits as to how high a spatial frequency can be transferred to the image (i.e. resolution). The effect of partial temporal coherence is manifested as a spread of focus, and that of partial spatial coherence as incident beam convergence. The effects of partial coherence can be included in HRTEM image simulations by summing images in real space, or by applying an appropriate transmission cross-coefficient (TCC) when computing the image intensity spectrum in reciprocal space. For linear images (from specimens thin enough to behave as weak phase objects), the TCC can be simplified and described in terms of "damping envelope" functions that multiply the usual phase-contrast transfer function. Several expressions for top-hat and gaussian models of convergence exist in the literature and in simulation programs. The standard deviations used to compute resolution damping can thus range over a factor of more than two for the same value of convergence. Results illustrate how differences in TCCs, and thus simulated images, can arise.

33823 R

M.A. O'Keefe and V. Radmilovic

The Effects of Small Crystal Tilts on Dynamical Scattering: Why Simulated Images are Thinner Than Experimental Ones

MSA Proc. 51, p.980 (1993).

Image simulations can accurately reproduce experimental HRTEM images only when imaging parameters are accurately known. These parameters include specimen properties such as unit cell structure, crystal orientation, and specimen thickness, as well as microscope parameters such as beam energy and coherence, objective aperture size, defocus and spherical aberration. Of these parameters, the most difficult to measure, and thus to include accurately, is the specimen thickness. In many investigations specimen thickness is treated as a disposable parameter; i.e. the experimental specimen thickness is not measured independently, but assumed to be the same as the best-match simulation. However, image character is not unique; i.e. the same image can be found at a different thickness if other conditions are allowed to vary within experimental error. For tilted crystals, images from thinner areas will retain the correct symmetry in first order, also the rate of image change with thickness will decrease; tilt will thus extend the range of thicknesses over which a "good" (or thin-crystal) image can be obtained (and may unknowingly be selected for this reason; crystallographic image processing often confirms the presence of small tilts in HRTEM images). The proportion of second-order contributions is lower from a tilted specimen, and the image appears to come from a thinner crystal. This effect is illustrated for aluminum in {001} orientation.

35341 No

U. Dahmen, N. Thangaraj, and R. Kilaas

Quantitative TEM Analysis of Microstructural Anisotropy

MSA Proc. 52, New Orleans, LA., 7/31-8/5/94 (submitted)

Preferred orientation of grain boundaries or interfaces in solids is an important indicator of anisotropy in boundary energy or kinetics. The present study is part of an ongoing investigation of faceting in thin films with the mazed bicrystal microstructure which possesses several unique features that are difficult to measure with standard parameters such as grain size distribution. One of the important characteristics of this microstructure is the degree and type of anisotropy.

35340 No

S.-Q. Xiao, S. Hinderberger, K.H. Westmacott, and U. Dahmen

Twin Induced Kinetic Shapes of Ge Precipitates in Al

MSA Proc. 52, New Orleans, LA., 7/31-8/5/94 (submitted).

Twinning plays an important role in the growth of Ge precipitates from solid solution in dilute Al-Ge Alloys. Previous work found a great variety of precipitate shapes and corresponding orientation relationships. At thermodynamic equilibrium only one of these has the lowest free energy, and is therefore the most stable shape. The symmetry of the equilibrium shape must conform to the bicrystal symmetry, i.e. the symmetry of precipitate and matrix superimposed by their orientation relationship. For a twinned precipitate the equilibrium shape is determined by the tricrystal symmetry, i.e. the intersection group of the symmetry of matrix, the precipitate and its twin. This shape is different from that of an untwinned precipitate. For the same reason, twinning can also change the precipitate-matrix interface structure, resulting in preferential growth along certain crystallographic directions. The effect induces non-equilibrium, growth or kinetic shapes. In this report a formation mechanism for the kinetic shapes of Ge precipitates due to twinning is proposed and preliminary TEM observations of the relationship between internal twinning and precipitate shape are presented.

35347 R

V. Radmilovic, R. Kilaas, and G. Thomas

Amorphization of $Al_{10}(V_x,Cr_{1-x})$ Intermetallic Phase

MSA Proc. 52, New Orleans, LA., 7/31-8/5/94 (submitted).

The stability of phases in alloy systems, including stability in irradiation environments, is *conditio sine qua non* of their engineering applications. Thus, investigations of different phenomena such as compositional variation, segregation, order/disorder transitions and amorphization in different phases under irradiation is of great importance.

35348 R

M.A. O'Keefe

Interpretation of HRTEM Images by Image Simulation: An Introduction to Theory and Practice

MSA Proc 52, New Orleans, LA., 7/31-8/5/94 (submitted).

High resolution transmission electron microscope (HRTEM) image simulation was conceived in 1970 in response to a referee's questioning of the interpretation of images of a niobium oxide. Two years later a suite of HRTEM image simulation programs had been established and shown to accurately reproduce experimental HRTEM images when imaging parameters were accurately known. These first simulated images proved that the original interpretation of the niobium oxide images was indeed correct. Once these programs were available, it was possible to explore HRTEM imaging parameters including specimen ionicity, validity of the projection approximation, and the resolution-limiting effects of incident-beam convergence. Over the twenty years since then, the range of uses of HRTEM simulation has continued to expand, as has the number of programs available. World-wide distribution of the SHRLI (simulated high-resolution lattice image) code inspired some researchers to produce new or modified simulation programs, and others to compare the results produced by these programs.

35350 No

L. Normand, A. Thorel, and Y. Montardi

Fantome: A Calculation of the Dielectric Function From the Plasmon Excitation

MSA Proc. 52, New Orleans, LA., 7/31-8/5/94 (submitted).

Electron Energy Loss Spectroscopy is now a well known method for chemical analysis (light elements especially), qualitative analysis of trace elements, EXELFS, etc. The low energy part of the spectrum can also be used in order to perform thickness evaluation and dielectric function determination. When EELS coupled with Transmission Electron Microscopy it presents the great interest of performing all measurements with a spatial resolution of the magnitude of the beam size. In the case of the dielectric function, we can then avoid any average effects due to macroscopic measurements. We then have access to the role of defaults, chemical heterogeneities, grain boundaries, anisotropy which can introduce major modifications in the macroscopic properties. The dielectric measurements are based on Kramers-Kronig analysis of the plasmon excitation: a program ("Fantome") has been written to process the EELS spectra. Results have been obtained on barium titanate.

35349 No

L. Normand, A. Thorel, and Y. Montardi

HREM Study of Ferroelectric Domain Wall in Barium Titanate

MSA Proc. 52, New Orleans, LA., 7/31-8/5/94 (submitted).

This study focuses on high resolution transmission electron microscopy of barium titanate in its tetragonal ferroelectric phase, and especially on the structure of domain walls. This phase is stable between about 0° C and 130° C. During cooling, at 130° C barium titanate changes from a cubic parraelectric phase to a tetragonal ferroelectric phase. In this phase the spontaneous polarization is along one of the six [001] pseudo-cubic directions. Two types of domains can be formed during the phase transition: 90° and 180° domains. In 90° domains the polarization is at 90° from the polarization of the next domain (exactly 2* ArcTan (a/c) if a and c are the lattice parameters). For these domains the domain walls are <110> type planes. In 180° domains the polarization is at 180° from the one in the next domain. 180° domain walls are <100> type plane and are assumed to be purely ferroelectric.

35351 R

V. Radmilovic, H. Gasteiger, and P. Ross

Structure and Chemical Composition of Pt-Ru Nanoparticle Supported on Carbon Black

MSA Proc. 52, New Orleans, LA., 7/31-8/5/94 (submitted).

The presence of nanoparticles in catalyst systems is essential because their large surface area increases the reaction rate of the catalyst. However, such a small size of the particles causes serious limitations in microstructural characterization, that could be overcome by high resolution electron microscopy (HREM), especially for particle morphology studies, presence of faults, etc. The present study uses HREM, microdiffraction and EDS techniques to characterize the Pt-Ru catalyst supported on amorphous carbon black. In order to get structural information from local region of single particle, optical diffraction has also been performed. HREM imaging allows the particle morphology and the presence of various structural defects to be revealed. To avoid contamination, microchemical analysis has been performed at -160° C, using cold stage beryllium holder. The fluorescence effect can be neglected.

35361 No

S. Hinderberger, S.Q. Xiao, K.H. Westmacott and U. Dahmen

Shape Training of Ge Precipitates in an Al-1.8 at% Ge Alloy

MSA Proc. 52, New Orleans, LA., 7/31-8/5/94 (submitted).

Ge precipitates in Al are known to form in a rich variety of shapes and orientation relationships. In this work it is shown that initial non-equilibrium shapes such as plates, laths, needles and tetrahedra can be induced to change to the equilibrium shape of an octahedron by proper temperature cycling. Analysis of this effect in bulk samples was complemented by direct observations of its mechanism during in-situ temperature cycling.

35395 No

S. Paciornik, R. Kilaas, J. Turner, and U. Dahmen

Pattern Recognition in HREM Analysis of Grain Boundary Structures

MSA Proc. 52, New Orleans, LA., 7/31-8/5/94 (submitted).

The present study focuses on an application of pattern recognition techniques to the detection of structural units in grain boundaries and in heterophase interfaces. It describes a simple means of extracting the essential characteristics of an interface from a high resolution image, to find the location, repeat distance and degree of similarity between such units and to sum them into an average unit with increased signal to noise ratio. A measurement of the discrimination between different crystallographic structures can also be obtained from a histogram of the processed image.

35360 No

S. Paciornik, U. Dahmen, I.G. Solorzano, and J.B. Vandersande

HREM Analysis of a Sigma 5 (210) Grain Boundary in Rutile

MSA Proc. 52, New Orleans, LA., 7/31-8/5/94 (submitted).

The present investigation combines HREM with image processing and simulation to determine both the atomic and the step structure of a near Sigma-5 (210) symmetrical grain boundary in TiO_2 (rutile), produce by melt growth from an oriented bicrystal seed. The results of this work leads to the surprising conclusion that there is a local non-stoichiometry at the interface with excess Ti ions, stabilized by a change to a +3 valence state. It is possible that an interfacial non-stoichiometry developed during the process of bicrystal preparation. This conclusion is further supported by the non-stoichiometry observed for the naturally occurring crystallographic shear faults in rutile.

35394 No reprints

M. Goldman, C.P. Burmester, L.T. Wille, and R. Gronsky

Strain and Domain Evolution in $YBa_2Cu_3O_z$

Philosophical Magazine Letters (submitted 3/24/94).

A Monte Carlo study of the time evolution of atomic positions and occupancies within the basal plane of $YBa_2Cu_3O_z$ is performed. The simulations are based upon an anisotropic Ising model, and, for the first time, include elastic interactions associated with continuous displacements at atoms within the basal plane. Samples quenched to temperatures below the disorder-order transition curve from the disordered, tetragonal state rapidly form orthorhombic domains separated by twin boundaries. The resulting microstructure is observed to coarsen and eventually anneal into a single domain that exhibits the experimentally observed superlattice reflections. Strain maps are used to elucidate and interpret these observations.

32855 R

G.C.L. Wong, D. Loretto, E. Rotenberg, M.A. Olmstead, and C.A. Lucas

CaF_2-Si(111) as a Model Ionic-Covalent System: Transition from Chemisorption to Epitaxy

Phy. Rev. B., Vol. 48, #8, p.5716 (1993).

The demands of chemisorption and epitaxy are quite different for electronically dissimilar systems. The transition between these two regions in CaF_2-Si(111) is studied with transmission electron microscopy and photoemission. Changes in the electronic structure of the evolving growth surface are expressed in the composite growth mode, a Stranski-Krastanow pathway to layer-by-layer growth, which begins with CaF_2 coherent island formation on a Si-CaF layer. After this transition, layer-by-layer CaF_2 homoepitaxy is possible even at room temperature, and the critical thickness can be extended.

35296 No

C.P. Burmester, L.T. Wille, and R. Gronsky

Microscopic Model and Computer Simulation of Detwinning in $YBa_2Cu_3O_x$

Physica C (submitted 3/2/94).

The results of Monte Carlo simulations of the detwinning of the high-temperature superconductor $YBa_2Cu_3O_x$ are reported. To study the effects of detwinning and the concomitant domain growth in this system, a sample is first produced having a representative domain structure using Monte Carlo simulation at fixed temperature and oxygen chemical potential based on an asymmetric two-dimensional Ising-model. The resulting microstructures typically consist of finely textured orthogonal domains indicative of a twinned structure. Next, a symmetry-breaking detwinning potential is imposed and the time evolution of the system is followed. At low temperatures or detwinning potentials only partial detwinning is typically achieved as the system is often frozen in 'glassy' domain structures, but at higher temperatures or detwinning potentials complete detwinning is attained. Domain kinetics is mapped out as a function of oxygen chemical potential and temperature and evidence is presented for an algebraic domain growth law of the form t^n with n between 0.33 and 0.75 depending on the control parameters.

33109 No

C.A. Lucas, G.C.L. Wong and D. Loretto

Structural Transitions of the CaF_2/Si(111) Interface

Phys. Rev. Lett., Vol. 70, #12, p.1826 (1993).

We have used x-ray reflectivity and transmission electron microscopy to study the CaF_2/Si(111) interface. The results are consistent with a reconstructed two-layer CaF interface which can be transformed to a different structure simply by increasing the thickness of the CaF_2 overlayer. We are able to reconcile previous measurements of the interface structure and gain insight into the rich variety of phenomena that may be observed at heteroepitaxial interfaces.

35378 No

C.A. Lucas, D. Loretto, and G.C.L. Wong

Epitaxial Growth Mechanisms and Structure of CaF_2/Si(111)

Physical Rev. B (submitted 3/94).

The early stages of interface formation between CaF_2 and Si(111) have been studied, in-situ, by a combination of reflection high energy electron diffraction, x-ray diffraction and core-level photoemission. The results are combined with ex-situ transmission electron microscopy to show that the initial growth mode changes from Volmer-Weber to Stranski-Krastanow, depending on the substrate temperature. The crossover is correlated with a submonolayer transition from the Si(111)-(7 x 7) to a (3 x 1) reconstruction. This is accompanied by fluorine dissociation at the interface. Both initial growth modes can lead to a uniform CaF_2 epilayer and subsequent growth on this surface is layer by layer. Using x-ray crystal truncation rod analysis, we have examined the CaF_2/Si(111) surface and interface structure. For films grown at temperatures above the (7 x 7) - (3 x 1) transition, the Ca atom in the CaF layer at the interface is located in a single T_4 bonding site. Finally, we have observed a structural transition at the interface from the as-grown structure to a root-3 R 30° reconstruction, which appears to be incommensurate. The dynamics of this transition and the possible mechanisms will be discussed.

34582 No

M. Goldman, C.P. Burmester, L.T. Wille, and R. Gronsky

Deformation Superstructures, Tweed, and Oxygen Vacancy Ordering Associated with Phase Transformations in $YBa_2Cu_3O_z$

Physical Review B (in press, 8/94).

A new theoretical technique is described, employing Monte Carlo simulation, which allows the investigation of strain effects associated with transformations in solids. The method applies a grand canonical stress ensemble in the study of elasticity during phase evolution in $YBa_2Cu_3O_z$ where both oxygen occupancy and atomic positions in the basal plane, as well as total sample volume, can vary. Quenching experiments yield both metastable square root $2a_o$ x square root $2a_o$ superstructures from short wavelength modulations and a "tweed" texture from long period <110> modulations of the ordered z = 7.0 compound.

---

un-numbered No

C.J.D. Hetherington and U. Dahmen

An Optical Moiré Technique for the Analysis of Displacements in Lattice Images

Proc. 10th Pfefferkorn Conf., p.405 (1993).

High resolution electron microscopy is a means for imaging not only the local structure at a defect or interface but also the displacement field in the surrounding lattice. However, in general it is difficult or tedious to analyze this field which can extend across the entire micrograph. The optical Moiré technique, which is based on interference effects between the experimental lattice image and an artificial reference lattice allows a rapid and accurate measurement of the displacement. Small violations of translation, rotation or mirror symmetries give rise to large changes in the periodicity or orientation of the moire´ pattern. The different types of patterns: simple rotation, simple parallel and "mixed", are then best interpreted by reference to reciprocal space vectors of the component lattices. Displacements in the experimental image revealed by the Moiré pattern represent displacements in the actual specimen under certain conditions. This technique therefore provides a means for detecting lattice defects and for measuring lattice rotations and rigid body shifts.

---

un-numbered No reprints

S. Schuppler, S.L. Friedman, M.A. Marcus, D.L. Adler, Y.-H. Xie, F.M. Ross, T.D. Harris, W.L. Brown, Y.J. Chabal, L.E. Brus, and P.H. Citrin

Dimensions of Luminescent Oxidized and Porous Silicon Structures

Physical Review Letters (accepted 3/18/94).

X-ray absorption measurements from H-passivated porous Si and from oxidized Si nanocrystals, combined with electron microscopy, ir-absorption, α-recoil, and luminescence emission data, provide a consistent structural picture of the species responsible for the visible luminescence observed in these samples. The mass-weighted average structures in por-Si are particles, not wires, with dimensions significantly smaller than previously reported or proposed.

33753 No

J.-O. Malm and M.A. O'Keefe

The Effect of Crystal Tilt on High Resolution Micrographs of Small Metal Particles

Proc. 45th SCANDEM, p.131 (1993).

The structures of small (1.5Å to 5.0 nm) metal particles have been studied extensively by high resolution transmission electron microscopy (HRTEM). When imaging particles of this size, it is not possible to use the tilting techniques (selected area diffraction) usually employed by the high resolution microscopist. Nevertheless, a surprisingly large proportion of particles show lattice fringes (often in two dimensions); the appearance of such fringes is usually interpreted as indicating that the particle is oriented close to a zone axis. This work shows that this assumption is sometimes optimistic and demonstrates the dangers in relying on the appearance of the image to decide the direction in which the particle is being viewed.

un-numbered No

F.M. Ross

Dynamic Observations of Pore Growth in Silicon

Proc. 5th Frontiers Conf., Oakland, CA., 6/21-6/24/94.

The recent (1990) discovery that anodically etched silicon can luminesce in the red part of the visible spectrum created an immense amount of interest in this fascinating material. Activity initially centered around the posibility of using porous silicon in electroluminescent devices, thereby finally achieving the aim of optoelectronic integration. However, this unusual material is also of interest a molecular sieves, filters and catalyst supports. These diverse applications depend on the microscopic details of the pores formed during the etching process, which as a function of the doping level and the etching conditions, can range from micron-sized straight channels of arbitrary aspect ratio to sub-nanometer, non-directional branched structures.

33428 No

C.P. Burmester, L.T. Wille, and R. Gronsky

Monte Carlo Simulation of Oxygen Ordering in the High Temperature Superconductor $YBa_2Cu_3O_x$

Proc. 6th SIAM Conf. on Parallel Processing, p.152 (1993).

The development of Monte Carlo single instruction multiple data (SIMD) parallel algorithms for the study of oxygen ordering in the basal plane of $YBa_2Cu_3O_x$ from first principles is described. In particular, implementation of the Ising model with short-range pair interactions on the SIMD architecture MasPar MP-1 (DEC mpp-12000) series of massively parallel computers is demonstrated. Special attention is given to methods which optimize processor array use and the particular pitfalls associated with parallel implementation of the Monte Carlo technique associated with the violation of ergodicity and coupling of the system Hamiltonian dynamics with the processor update period.

33427 No

C.P. Burmester, L.T. Wille, and R. Gronsky

Computer Simulations of Growth Mechanisms in Y-Ba-Cu-O Thin Films

Proc. 5th Int'l. Symp. on Superconductivity, p.883 (1993).

The growth of epitaxial thin films of $YBa_2Cu_3O_7$ is studied by means of computer simulation of the deposition and diffusion of Y, Ba, and Cu oxide particles. The evolution process is modeled by means of a three-step Monte Carlo technique incorporating one sorption deposition mode and two modes of film annealing addressing surface and bulk diffusion. A systematic study of the effects of deposition rate and substrate temperature during in-situ film fabrication reveals that the kinetics of film growth can readily dominate the structure formation of the thin film leading to dramatic morphological transitions as a function of deposition conditions alone.

33886 No

F. Ross, R. Hull, D. Bahnck, J. Bean, L. Peticolas, C. King and R. Kola

Changes in Electrical Device Characteristics During the Formation of Dislocations *in situ* in the TEM

Proc. 8th Oxford Conf. on Microscopy of Semiconducting Mat., # 134, p.245 (1993).

By adding electrical connections to a specimen heating holder for a transmission electron microscope, we have measured the characteristics of electronic devices such as diodes while they remain under observation in the microscope. We have made electron-transparent specimens from metastable GeSi/Si p-n junction diodes and introduced dislocations by heating *in situ*. The combination of electrical measurement and real-time observation of dislocation formation allows us to examine the electrical properties of dislocations in individual devices and the influence of defects on device performance.

un-numbered No

Kenneth H. Downing, Michael A. O'Keefe, and Hans-Rudolph Wenk

Oxygen Contrast in Ionic Structures: 3D Electron Crystallography of YBCO.

Proc. ICEM 13, (in press, July, 1994)

Electron crystallography employs methods of crystal structure determination based on electron interaction with crystals. We report on direct phase determination and reconstruction of the structure of the orthorhombic YBCO ($YBa_2Cu_3O_{7-\delta}$) high temperature superconductor from high resolution images in five different directions. A polycrystalline sample of YBCO was sectioned, ion thinned and carbon coated. High resolution images were obtained with the JEOL ARM-1000 atomic resolution microscope, operated at 900 keV with a spherical aberration of 2mm and a point-o-point resolution of 1.6Å. The 3D reconstruction clearly indicates cation positions and may show strong effects of oxygen ionicity.

33157 P

M.A. O'Keefe

Using Coherent Illumination to Extend HRTEM Resolution: Why we Need a FEG-TEM for HREM

Proc. Microstructures of Materials Conf., p.121 (1993).

The resolution of a high-resolution transmission electron microscope (HRTEM) has traditionally been defined in terms of its Scherzer resolution limit at optimum defocus. However, even beyond the Scherzer limit, spatial frequencies can be transferred from the specimen to the image, out to the so-called information limit of the electron microscope. The information limit of the HRTEM is determined by the degree of energy spread in the electron beam used to illuminate the sample. Since a HRTEM equipped with a field-emission gun (FEG) will produce an electron beam of high coherence with little energy spread, it can achieve an improved information limit, and can thus be used to produce through-focus series of images containing information well beyond its nominal (Scherzer) resolution limit. Suitable computer processing of such series of images can produce composite images at resolutions approaching the microscope information limit. For such a FEG-TEM, combined with suitable computer image processing, resolution can approach 1Å.

---

un-numbered No

M.A. O'Keefe and V. Radmilovic

Specimen Thickness is Wrong in Simulated HRTEM Images

Proc. ICEM 13, Paris, France, 7/17-7/22/94.

Simulated high-resolution transmission electron microscope (HRTEM) images can accurately reproduce experimental HRTEM images only when imaging parameters are accurately known. The most difficult parameter to measure accurately is the specimen thickness. In matches between experimental and simulated HRTEM images, specimen thickness is often regrettably treated as a disposable parameter; i.e. the experimental specimen thickness is not measured, but assumed to be the thickness at which the simulated image best matches the experimental one. Such a procedure can result in seriously-underestimated specimen thicknesses, since a simulated crystal must always be thicker than an experimental one to produce the same image. Sometimes the matching thickness at the known defocus appears ridiculously small and a greater thickness is selected (incorrectly) by taking advantage of the trade-off between objective defocus and specimen thickness. With increasing specimen thickness, simulated images attain a specific image character faster than do experimental ones because simulated scattering is more dynamical, since simulated specimens are positioned exactly on-axis and experimental specimens are not.

33474 No

U. Dahmen

Split Reflections from Broken Mirrors: Symmetry-Breaking in the Making of Materials Microstructures

Proc. Microstructures of Materials Conf., p.24 (1993).

The symmetry underlying the development of microstructure in materials is a global property with great practical uses in the design and analysis of precipitate distribution and morphologies, orientation relationships between crystals, properties of interfaces and textures and topographies of microstructures.

un-numbered No

S. Im, J. Washburn, R. Gronsky, and K.M. Yu

Defect Minimized SiGe Layer Using Ion Beam Synthesis

Proc. MRS, Vol. 279 p.249 (1993).

Ion beam synthesis for SiGe layers was performed to study the end of range (EOR) defects and strain-induced dislocations. High Ge doses of 5 x $10^{16}/cm^2$, 3 x $10^{16}/cm^2$ and 2 x $10^{16}/cm^2$ at 120 keV were implanted to obtain 12 at%, 7 at% and 5 at% of Ge peak concentrations respectively. RBS spectra show a projected range (R_p) at a depth of 65nm and an amorphous thickness of 170 nm on a wafer with 12 at% of Ge peak concentration. Ge ion implantation was performed both at room temperature (RT) and at liquid nitrogen temperature (LNT), in order to investigate the effect of implantation temperature on reducing EOR defect density. Solid phase epitaxial (SPE) annealing for all SiGe layers was done in nitrogen ambient at 800° C. The EOR defect density is considerably reduced by LNT implantation and the strain-induced dislocations have a threshold Ge peak concentration (about 6 at%) for their abrupt generation. For SiGe layer with 12 at% Ge peak concentration, the amorphous-crystalline (a/c) interfacial morphology changes from a planar interface into a faceted interface during SPE growth at 550° C.

---

un-numbered No

S. Im., J. Washburn, R. Gronsky, N.W. Cheung, K.M. Yu, and J.W. Ager

Reducing Dislocation Density by Sequential Implantation of Ge and C in Si

Proc. MRS, Vol. 298, p.139 (1994).

Carbon implantation was performed after high dose Ge implantation into [100] oriented Si substrates to study the effect of sequential implantation on dislocation nucleation. When the nominal peak concentration of implanted C is over 0.55 at%, dislocations in the SiGe layer containing C are considerably reduced in density after solid phase epitaxial (SPE) annealing at 800° C for 1 hour, compared to the SiGe layer without C. These results suggest that during annealing, C atoms compensate the Ge-induced misfit strain which causes dislocation generation in the region of peak Ge concentration. Channeling spectra obtained by RBS analysis show only 5% to 6% minimum back scattering yield as C atoms suppress the dislocation generation.

33478 P

F.M. Ross, R. Hull, D. Bahnck, J.C. Bean, L.J. Peticolas, R.R. Kola and C.A. King

Changes in Electronic Device Properties During the Formation of Dislocations

Proc. MRS, Vol. 280 (in press, 1994).

We describe the results of an investigation into the formation and properties of dislocations in electronic devices. We have made electron transparent specimens from metastable GeSi/Si p-n junction diodes and introduced dislocations into the devices by heating *in situ* in the electron microscope. A modification made on the specimen holder for our microscope enables us to measure the characteristics of these devices while they remain under observation in the microscope. We can therefore observe the changes in the electrical properties of the devices as dislocations form. We confirm that the introduction of dislocations has a deleterious effect on parameters such as the reverse leakage current through a diode. However, the magnitude of the effect we observe cannot be explained by a generation-recombination process and instead, we suggest a model based on the creation of point defects or the diffusion of metals during the formation of dislocations. We also consider the kinetics of dislocation formation, and in particular how the extent of dislocation formation in a device depends on the subsequent processing steps which it undergoes.

---

unnumbered No

R.F. Marks, R.F.C. Farrow, G.R. Harp, S.S.P. Parkin, T.A. Rabedeau, M.F. Toney, A. Ceboliada, N. Thangaraj, and K.M. Krishnan

Giant Magnetoresitance and Structure of Phase Segregated Metals

Proc. MRS, Vol. 313, p.411 (1993).

Giant magnetoresistance, GMR, in thin metal films elicits attention due to its technological potential as well as its relevance to theory of exchange coupling. Epitaxial, phase-segregated ferromagnet/paramagnet mixtures have been grown by UHV evaporation. Such films show spontaneous formation of ferromagnetic clusters, and large values of GMR (40% at room temperature) as grown. The growth of Co-Cu, Co-Ag, Fe-Ag, and permalloy-Ag films are described. Structural analysis by grazing-incidence small angle x-ray scattering (GISAXS) provides a measure of cluster size and characteristic spacing. Effects of growth temperatures and subsequent annealing on GMR and film structure are described. Preliminary results of TEM examination of (001) Fe-Ag and Co-Ag granular films are presented for the first time.

34856 P

F.M. Ross, R.R. Kola, R. Hull, and J.C. Bean

Microstructural Evolution and Stress Relaxation in Sputtered Tungsten Films

Proc. MRS, Vol. 318 (in press, 1994).

We have investigated the relationship between microstructure and stress in very thin sputtered W films. We discuss features of the microstructure, in particular the presence of voids in compressively stressed films, in terms of the evolution of the structure from a metastable β-phase. By developing a novel specimen geometry for the transmission electron microscope (TEM), we present dynamic observations of the β-W->α-W transformation.

34934 R

N. Thangaraj, S. Hinderberger, K.H. Westmacott, and U. Dahmen

Thermal Stability of Epitaxial Al/Si Interfaces

Proc. MRS, Vol. ULSI-IX, p.247 (1994).

The morphological stability of epitaxial Al/Si interfaces during interdiffusion has been studied by electron microscopy. It was found that Si dissolution in the Al film during annealing and Si precipitation during cooling were both heterogeneous processes, forming Al spikes in the Si substrate and Si precipitates on the Al film, respectively. Dynamic observations during in-situ annealing of cross section samples in an electron microscope revealed that spikes nucleated at the junction of Al grain boundaries (gb's) with the Si substrate. Some special grain boundaries did not nucleate spikes. Ex-situ heat treatments showed that the extent and the shapes of spiked regions depended on the interfacial crystallography. From scanning (SEM) and cross-sectional transmission electron microscopy (XTEM) studies, it was found that the Al spikes on Si(100) substrates were hemispherical whereas spikes on Si(111) substrates were disc-shaped.

35156 R

M.A. O'Keefe, K.H. Downing, H.-R. Wenk, and H. Meisheng

3-D Imaging of Crystals at Atomic Resolution

Proc. MRS, Vol. 332 (in press, 1994).

Electron crystallography has now been used to investigate the structures of inorganic materials in three dimensions. As a test of the method, amplitudes and phases of structure, factors were obtained experimentally from high resolution images of staurolite taken in a number of different projections. From images in five orientations, a three-dimensional Coulomb potential map was constructed with a resolution of better than 1.4Å. The map clearly resolves all the cations (Al, Si, Fe) in the structure, and all of the oxygen atoms. This method promises great potential for structure determinations of small domains in heterogeneous crystals which are inaccessible to x-ray analysis. Three-dimensional structure determinations should be possible on small domains only approximately 10 unit cells wide, and may resolve site occupancies in addition to atom positions. Given a microscope stage with a suitable range of tilt and enough mechanical stability, the method could also be applied to small crystalline particles larger than about 50Å to 100Å. In addition, with sufficient computing power, it may be possible to apply the method to derive the two-dimensional structure of periodic defects.

---

un-numbered No

R.S. Kedia, T.M. Lillo, Q. Horn, M.R. Plichta, and S.A. Hackney

Edge Instabilities in Thin Plates with Spatial Variations in Thickness

Scripta Met. et Mat., Vol. 28, p.269 (1993).

The morphological stability of two dimensional structures has far-reaching consequences in a variety of materials problems. For example, the time dependent behavior of lamellar composite materials and thin coatings at elevated temperature can be directly related to the morphological integrity of the two dimensional structure. Time dependent behavior can be expected when the two dimensional morphology is not the equilibrium morphology and a thermodynamic driving force exists for the thin layer to undergo a morphological change to a structure with a smaller surface area to volume ratio. In many cases, the change in morphology occurs by a diffusional instability at the edges of two dimensional structures. The edge instabilities of two dimensional structures have been studied in relation to microcrystalline thin film stability, thin plate stability, intergranular film stability, and crack healing in brittle materials.

un-numbered No

E. Goo, A. Murthy, and C.J.D. Hetherington

Preferential Amorphitization of NiTi Alloys at Twin Boundaries by Electron Microscopy

Scripta Met. et Mat., Vol. 29, p.553 (1993).

NiTi alloys will amorphitize under electron irradiation. Amorphitization occurs quite readily for electrons with energies greater than 1 MeV. The mechanism for amorphitization is believed to be displacement damage. This paper reports the preferential amorphitization at deformation twin boundaries in NiTi alloys by electron microscopy.

33720 P

S. Paciornik, R. Kilaas and U. Dahmen

Assessment of Specimen Noise in HREM Images of Simple Structures

Ultramicroscopy, Vol. 50, p.255 (1993).

Displacements of image spots representing atomic columns in a high resolution image may be due either to displacements of atomic columns or to specimen noise. The effect of specimen noise on the accuracy with which an atomic column can be located is assessed by evaluating the root mean square deviation of the intensity center of mass of image dots. Optimized methods for experimental assessment of this effect are developed and applied to simulated and experimental images.

34392 P

F.M. Ross, J.M. Gibson, and R.D. Twesten

Dynamic Observations of Interface Motion During the Oxidation of Silicon

Surface Science (in press, 1994).

We describe real time observations of the behavior of the silicon-oxide interface during oxidation in situ in an ultra high vacuum transmission electron microscope. We have formed clean, flat Si (111) surfaces by heating under UHV and allowed oxidation or oxygen etching to proceed in the microscope. We have examined the kinetics of both the oxidation and etching reactions using an imaging technique based on the use of forbidden reflections in silicon. We find that oxidation to form SiO_2 occurs by the reaction of discrete monolayers with no flow of surface steps. This is in dramatic contrast to oxygen etching, during which the volatile oxide SiO evaporates preferentially from step edges.

32290 P

B. Zhang, K.M. Krishnan and R.F.C. Farrow

Crystallography of Co-Pt Multilayers and Nanostructures

Ultramicroscopy, Vol. 51, p.298 (1993).

Atomically engineered nanostructures and multilayers of Co-Pt exhibit strong perpendicular anisotropy. This unique property, that determines their potential as a magneto-optic recording media, is dependent on a variety of microstructural parameters that include the overall crystallography, thickness of the layers, orientation, defect formation, interface reactions, etc. A series of Co-Pt multilayer samples with different thickness of the Co layer were studied by electron diffraction. It has been determined that the Co layers persist in the fcc structure up to a thickness of 50Å. As the thickness is varied from 3Å to 50Å in the multilayers, the Co film gradually relaxed to its bulk lattice parameter. (111) twinning and lattice strain at the interfaces between Pt and Co layers are also observed. The symmetry forbidden reflections observed at 1/3 {224} positions in [111] zone diffraction patterns of the multilayer are due to (111) twinning and compositional modulations along the multilayer growth direction.

un-numbered No

S.A. Hackney, T.M. Lillo, R.S. Kedia, Q.C. Horn, and M.R. Plichta

Edge Instabilities in Thin Plates Studied by in situ Transmission Electron Microscopy

Ultramicroscopy, Vol. 51, p.81 (1993).

The morphological instability of thin foil edges at elevated temperature is studied by in situ TEM. Quasi-periodic instabilities in the edge profile are observed with a distinct growth direction perpendicular to the original edge. The rods are then observed to undergo spheroidization. The use of in situ techniques allows the direct study of the thickness changes associated with the formation and propagation of this instability. Such examination of the details of the thickness changes is critical to a full understanding and perhaps the control of the phenomenon.

Please send a reprint of the paper(s):

Number	Author(s)	Title

Name_____ Date_____

Affiliation_____

Address_____

_____

Please send a reprint of the paper(s):

Number	Author(s)	Title

Name_____ Date_____

Affiliation_____

Address_____

_____

National Center for Electron Microscopy
U.C. Lawrence Berkeley Laboratory
1 Cyclotron Rd. Building 72
Berkeley CA 94720

National Center for Electron Microscopy
U.C. Lawrence Berkeley Laboratory
1 Cyclotron Rd. Building 72
Berkeley CA 94720

DISCLAIMER

This document was prepared as an account of work sponsored by the United States Government. Neither the United States Government nor any agency thereof, nor The Regents of the University of California, nor any of their employees, makes any warranty, express or implied, or assumes any legal liability or responsibility for the accuracy, completeness, or usefulness of any information, apparatus, product, or process disclosed, or represents that its use would not infringe privately owned rights. Reference herein to any specific commercial product, process, or service by its trade name, trademark, manufacturer, or otherwise, does not necessarily constitute or imply its endorsement, recommendation, or favoring by the United States Government or any agency thereof, or The Regents of the University of California. The views and opinions of authors expressed herein do not necessarily state or reflect those of the United States Government or any agency thereof or The Regents of the University of California and shall not be used for advertising or product endorsement purposes.

Lawrence Berkeley Laboratory is an equal opportunity employer.

National Center for Electron Microscopy
Lawrence Berkeley Laboratory
University of California
Berkeley, Ca 94720